


Genomic potential for mercury biotransformation in marine sediments across marginal slope to hadal zone

Received: 23 August 2024

Accepted: 29 August 2025

Published online: 30 September 2025

 Check for updatesZhuobo Li¹, Taoshu Wei², Lisheng He², Haifeng Qian³, Yong-Guan Zhu⁴ & Yong Wang^{1,5} 

Mercury accumulates in the deep sea, but its ecological impact on deep-sea ecosystems remains poorly understood. We conduct an analysis of 32 sediment cores, comprising 101 layers for the study of metagenomes, and additional 41 global reference sediment metagenomes. These sediment cores are collected from two deep-sea regions: the South China Sea and Mariana Trench, followed by revealing high mercury accumulation in the South China Sea. In these metagenomes, we find that the mercury methylation genes *hgcAB* are abundant in marginal seas but negligible in open oceans. Genomics result indicates that some Hg-methylating microorganisms affiliated with Desulfobacterota, Spirochaetota, and Zixibacteria in the deep-sea sediments encode MttB, the sole corrinoid-dependent methyltransferase identified in these taxa, which may interact with HgcA to transfer methyl groups from possibly osmolyte-derived trimethylamine for methylation. The demethylation gene *merB* is widely distributed and exhibits higher abundance in the open ocean. Moreover, we identify a large number of novel Hg demethylating taxa that are associated with horizontal transfer of the *merB* gene potentially involving methane generation. Our results expand the diversity of Hg-transforming taxa and reveal their unique ecophysiological adaptations in deep-sea sediments.

Mercury (Hg), emanating from both natural and anthropogenic sources, infiltrates the marine environment through a variety of pathways¹. It is delivered to the marine via atmospheric deposition², river outflow³, submarine groundwater discharge⁴, and the input from deep-sea hydrothermal vents⁵. In particular, rivers transport a large amount of mercury to estuaries and marginal seas, and only a small fraction is transported to open ocean areas⁶. Deposited Hg is influenced by long-range atmospheric transport and ocean current circulation⁷.

Hg is mainly found in the oceans as inorganic Hg(II) or Hg(0), but microorganisms can methylate Hg(II) to produce methylmercury (MeHg), and photochemical and microbial processes can break down MeHg into Hg(II) or Hg(0)⁸. Hg is a highly toxic metal and has attracted

increasing public attention over the past few decades^{9–11}. Methylmercury (MeHg) is considered a potent neurotoxin that can bioaccumulate through food webs with potentially harmful effects on human health^{10,12}. Human exposure to MeHg includes consumption of contaminated marine fish and rice^{13,14}.

Methylation of mercury and demethylation of methylmercury are mainly achieved by microbial biotransformation^{15,16}. The formation of MeHg by microorganisms is mediated by functional proteins encoded by the two-gene cluster consisting of *hgcA* and *hgcB*¹⁷. The *hgcA* gene encodes a corrinoid protein that acts as a methyl carrier, and the *hgcB* gene encodes a ferredoxin protein that participates as an electron donor in the reduction of corrinoid cofactors¹⁷. It is widely recognized

¹Institute for Ocean Engineering, Shenzhen International Graduate School, Tsinghua University, Shenzhen, China. ²Institute of Deep Sea Science and Engineering, Chinese Academy of Sciences, Sanya, China. ³College of Environment, Zhejiang University of Technology, Hangzhou, China. ⁴Key Lab of Urban Environment and Health, Institute of Urban Environment, Chinese Academy of Sciences, Xiamen, China. ⁵Shenzhen Key Laboratory of Advanced Technology for Marine Ecology, Shenzhen International Graduate School, Tsinghua University, Shenzhen, China. ✉e-mail: wangyong@sz.tsinghua.edu.cn

that MeHg is produced primarily by anaerobic microorganisms in the environment, including sulfate-reducing bacteria (SRB), iron-reducing bacteria and methanogens¹⁸. In addition to Hg methylation, methylmercury demethylation also plays a key role in the global Hg cycle. Biological demethylation of methylmercury is mainly a process of microorganisms utilizing the *mer* operon for mercury resistance and detoxification¹⁹. This process is primarily catalyzed by the alkylmercury lyase encoded by the *merB* gene, which cleaves the C-Hg bond in MeHg to CH_3^- and Hg(II) . Subsequently, the reduction of Hg(II) to Hg(0) is catalyzed by the mercury reductase MerA encoded by the *merA* gene. The *hgcAB* and *merAB* gene pairs provide key molecular biomarkers for mercury and methylmercury biotransformation studies. However, current studies on mercury cycling in the deep ocean are primarily concerned with assessing mercury concentrations in the deep ocean, pinpointing mercury sources, and analyzing research conducted in cold seep areas^{20–22}. In the wider deep ocean, the distribution pattern and microbial regulators of mercury cycling are uncertain yet, and the specificity of mercury cycling in the high-pressure, oligotrophic deep ocean remains to be investigated.

In this study, we collect sediment samples from the South China Sea (SCS), Bashi Channel (BS) and Mariana Trench (MT) for metagenomics and metatranscriptomics studies. The relative abundance of genes mediating Hg transformation indicates that methylation is present only in the marginal seas, while demethylation is widespread. In addition, the process of mercury methylation potentially using osmolyte-derived trimethylamine in deep-sea sediments is characterized by unique deep-sea adaptations, and we also identify a large number of novel demethylating taxa.

Results

Microbial novelty, biodiversity and geochemistry of deep-sea sediments

In the South China Sea and nearby areas, thirteen sediment cores were collected, comprising six cores from the slope of the South China Sea margin (SCS_S), three cores from the central part of the South China Sea Basin (SCS_B), and four cores from the vicinity of the Bashi Channel. In addition, 19 sediment cores were retrieved from the open ocean region, consisting of 6 cores from the northern slope of the Mariana Trench (MTS, < 4000 m depth) and 13 cores from the Challenger Deep of the Mariana Trench (MTCD, > 5000 m depth) (Fig. 1a and Supplementary Data 1). The 32 sediment cores are scattered over a depth range of 1087 m to 10,909 m, from the marginal slopes of South China Sea to the deepest region of the ocean (Challenger Deep of Mariana Trench) (Fig. 1b). In addition, the 41 metagenomes downloaded from NCBI Sequence Read Archive were from samples collected at depths ranging from 100 m to 9161 m (Fig. 1b and Supplementary Data 2). Total mercury concentrations were measured in 21 samples (Supplementary Data 3), which indicates higher concentrations in the samples from the marginal slope represented by the Bashi Channel samples (Fig. 1c and Supplementary Data 3). In sediment cores from the marginal slope, deeper layers generally exhibited higher methylmercury content, whereas surface layers of Challenger Deep of the Mariana Trench in the open ocean displayed higher methylmercury concentrations (Supplementary Data 3). The mean proportion of methylmercury in total mercury across sampling sites ranged from 63.25% to 82.06%. The NH_4^+ and PO_4^{3-} concentrations at Bashi Channel (0.19–2.02 mg L^{-1} ; 0.03–0.40 mg L^{-1}) and South China Sea slope (0.10–1.47 mg L^{-1} ; 0.18–0.21 mg L^{-1}) were comparatively higher than the other sites, according to pore water nutrient analyses of 52 sediment layers from 32 cores (Supplementary Data 4). The sulfate concentration was highest in BS2 (9595.50–9688.00 mg L^{-1}) and lowest in SCS5 (1470.84 mg L^{-1}), with variations likely influenced by the combined effects of location and depth (Supplementary Data 4). In contrast, Fe^{3+} concentrations were almost all below the detection limit (0.125 mg L^{-1}), except for 56 mg L^{-1} in SCS4-3.

Alpha diversity indices such as ACE, Chao1 and Shannon values calculated using metagenomic 16S rDNA Illumina tags (miTag) for the V4 region were highest in the Bashi Channel, followed by the South China Sea Basin and South China Sea slope (Supplementary Fig. 1a–c). The inverse Simpson values followed a similar trend, with Bashi Channel, South China Sea Basin and South China Sea slope being higher in the marginal sea than in the open ocean for northern slope of the Mariana Trench and Challenger Deep of Mariana Trench (Supplementary Fig. 1d). These findings suggest that the diversity of microorganisms in the marginal sea sediments was higher compared to the northern slope of the Mariana Trench and Challenger Deep of Mariana Trench. The percentage of novel 16S miTags (determined as < 97% identity to references in the SILVA 138 SSU database) recovered from the metagenomes was significantly higher in Bashi Channel (27.28%; $n = 12$) and Challenger Deep of Mariana Trench (25.99%; $n = 37$) (Wilcoxon test, $p < 0.001$) than that of other sites (Fig. 2a and Supplementary Data 5). We also calculated microbiome novelty scores (MNS) for all sediment samples to evaluate microbiome novelty (Fig. 2b). 84.16% of all the samples had an MNS value > 0.12, which is the cutoff value for the novel microbiome²³ (Fig. 2b and Supplementary Data 5). Similarly, the MNS of the Bashi Channel and Challenger Deep of the Mariana Trench samples was relatively higher, compared with the South China Sea and the northern slope of the Mariana Trench samples (Fig. 2b). The relative abundances of prokaryotic species were then predicted using 8865 ribosomal protein S3 gene (*rpS3*) sequences identified in the reads for the individual metagenomes. The principal coordinate analysis (PCoA) showed a strong similarity between the *rpS3*-based prokaryotic community structures of the northern slope of the Mariana Trench and South China Sea Basin sites (Supplementary Fig. 2), as well as between those of the marginal slope sites of the South China Sea slope and Bashi Channel. The canonical correspondence analysis (CCA) results suggest a potential linkage of the prokaryotic microbial communities with TN at the South China Sea slope and Bashi Channel sites, and with PO_4^{3-} , NH_4^+ and NO_2^- at the northern slope of the Mariana Trench and South China Sea Basin sites (Fig. 2c).

Genome reconstruction and mercury transformation in the deep-sea sediments

To investigate the microbe-mediated Hg transformations in sediments, 1672 Metagenome-Assembled Genomes (MAGs) with > 50% completeness and < 10% contamination were identified in all sediment metagenome datasets. To eliminate redundancy, we obtained 1476 MAGs after removal of duplicates in these MAGs (Supplementary Data 6). Proteobacteria (25.95%), Chloroflexota (12.94%), Planctomycetota (8.47%), Bacteroidota (4.54%), and Thermoproteota (4.47%) were the most representative phyla. The *hgcAB* and *mer* genes involved in mercury biotransformation were identified within the open reading frames of MAGs and assembled contigs by hmmsearch and KofamScan against the Hg MATE database and KEGG Ortholog database, respectively. The levels of these genes were quantified in each sample based on coverage by sequencing reads (Supplementary Data 7). The results showed that the relative abundance of *hgcAB* was lower than that of *mer* genes (Supplementary Fig. 3a, b). Within the *mer* operon, the relative abundance of *merT* is higher, followed by *merR* (Supplementary Fig. 3a, b). The samples were divided into two groups based on their locations: the marginal sea and the open ocean. The CPM (gene copy number per million reads) values for all genes were higher in the open-ocean group, with the exception of two gene pairs: the *hgcAB*, which had higher CPM values in the marginal sea group (Two-sided Wilcoxon test, $p < 0.05$), and the *merCF*, which showed no significant difference between the two groups (Fig. 3a). Hence, both mercury methylation, demethylation, reduction, transport and regulatory genes were frequently detected in the deep-sea sediments, but they showed distinct region- or depth-dependent distributions. The transcriptomic data of the three Challenger Deep of Mariana Trench

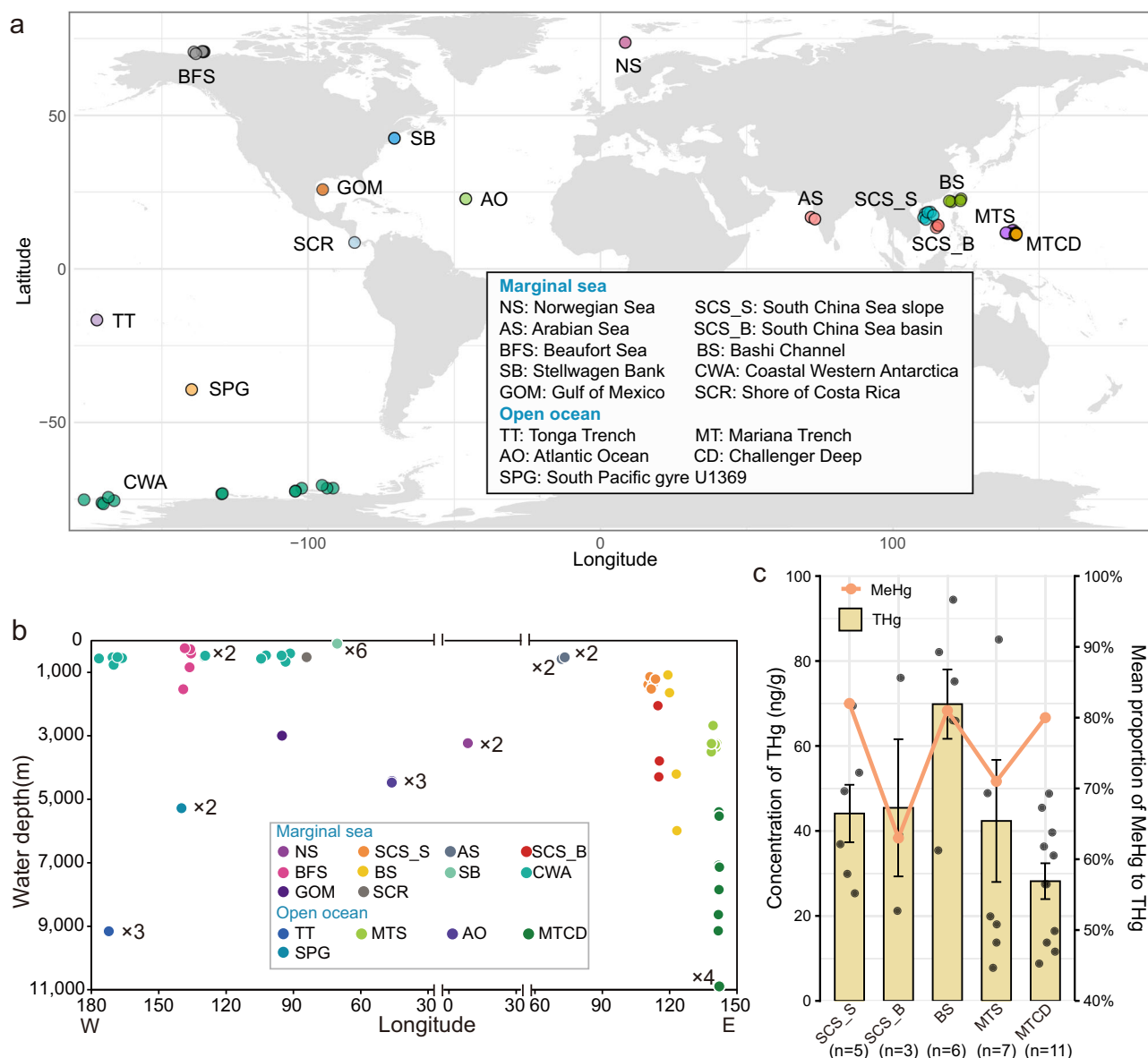


Fig. 1 | Geographical distribution and mercury concentrations of study sites.

a Geographical distribution of the 15 stations in this study. The sediment samples from the five regions (South China Sea slope, South China Sea Basin, Bashi Channel, northern slope of the Mariana Trench, Challenger Deep of the Mariana Trench) were used for this study. The metagenomic data for the sediment cores obtained

from ten additional regions were downloaded from the NCBI database. **b** Depth distribution of the sediment samples. **c** Total mercury (THg) and methylmercury (MeHg) concentrations in samples. The error bars represent the standard error of the mean. Source data are provided as a Source Data file.

samples showed that all of these genes associated with Hg transformation were expressed, with the exception of the Hg methylation gene *hgcB* and the regulatory gene *merD* (Fig. 3b and Supplementary Data 8). *merT* had the highest transcriptional levels among these genes, followed by the regulatory gene *merR* (Fig. 3b).

The survey of Hg biotransformation genes in all MAGs showed that *merT*, which encodes a mercuric ion transport protein, was widely distributed among microbial taxa in deep-sea sediments (on average, South China Sea slope: 25.90%; South China Sea Basin: 25.69%; Bashi Channel: 23.60%; northern slope of the Mariana Trench: 21.78%; Challenger Deep of Mariana Trench: 36.41%) (Supplementary Fig. 4). In addition, the mercury methylation genes *hgcAB* were found mainly in MAGs of the marginal slope group, and in the open-ocean group only in Nitrospinota (B20T3L14), Nitrospirota (B48T1B8, B18T1B5) and Chloroflexota (B27T3L14) of the Challenger Deep.

Diversity and distribution of putative Hg-methylating micro-organisms in deep-sea sediment

A total of 2163 *hgcA* sequences with a conserved motif (N(V/I)WCA(A/G)) were identified in assemblies from all sediment layers. The analysis of *hgcA* gene abundance showed that *hgcA* abundance detected in the marginal-sea group was greater than that of the open-ocean group at the different sampling depths studied, and the number of *hgcA* found in the deeper layers of the marginal-sea group was higher than that of its surface layers, suggesting that the methylators in the deeper layers of the marginal slopes might be of higher diversity and abundance (Supplementary Fig. 5). To further investigate the diversity of the mercury methylators, we conducted a detailed investigation of the methylator composition in the sediment cores. A total of 83 dereplicated MAGs with conserved *hgcA* (N(V/I)WCA(A/G), Supplementary Fig. 6a) and *hgcB* (CX2CX2CX3C, Supplementary Fig. 6b) motifs were identified in the

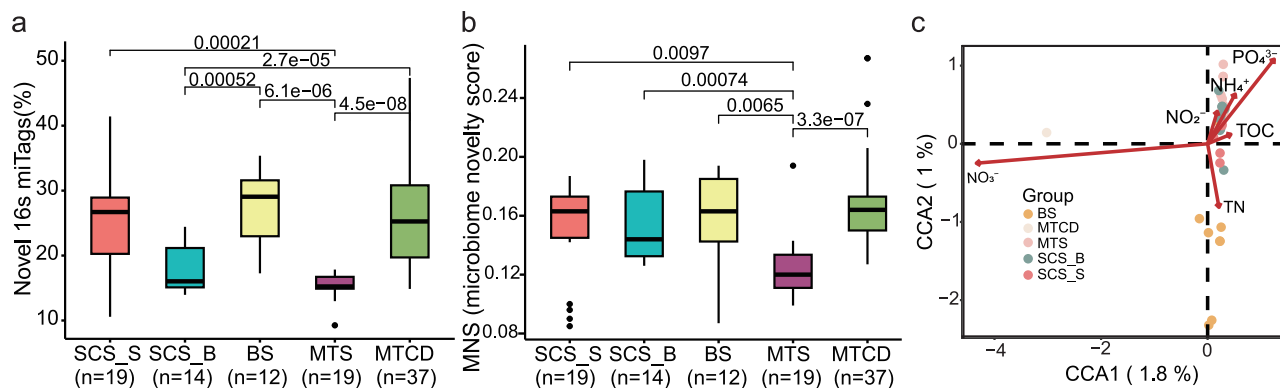


Fig. 2 | Novelty evaluation and CCA analyses of prokaryotic community structures. **a** Percentage of novel 16S miTags at different stations in reference to the SILVA 138 SSU database (p -values were estimated using the two-sided Wilcoxon test for pairwise comparisons). **b** Estimate of microbiome novelty scores (MNS) at different stations (p -values were estimated using the two-sided Wilcoxon test for pairwise comparisons). **c** CCA analysis of prokaryotic community structures of marine sediments and associated environmental factors. The relative abundances of *rpS3* sequences from different metagenomes were used for the CCA analysis,

along with environmental factors. In the box plot (**a**, **b**), center lines indicate median values. The lower and upper bounds represent 25th and 75th percentiles, respectively. The lower/upper whiskers represent minima/maxima no further than 1.5 times the interquartile range from the hinge, and the points falling outside of the whiskers represent the outliers. *SCS_S* South China Sea slope; *SCS_B* South China Sea basin; *BS* Bashi Channel; *MTS* Mariana Trench slope; *MTCD* Challenger Deep of Mariana Trench. Source data are provided as a Source Data file.

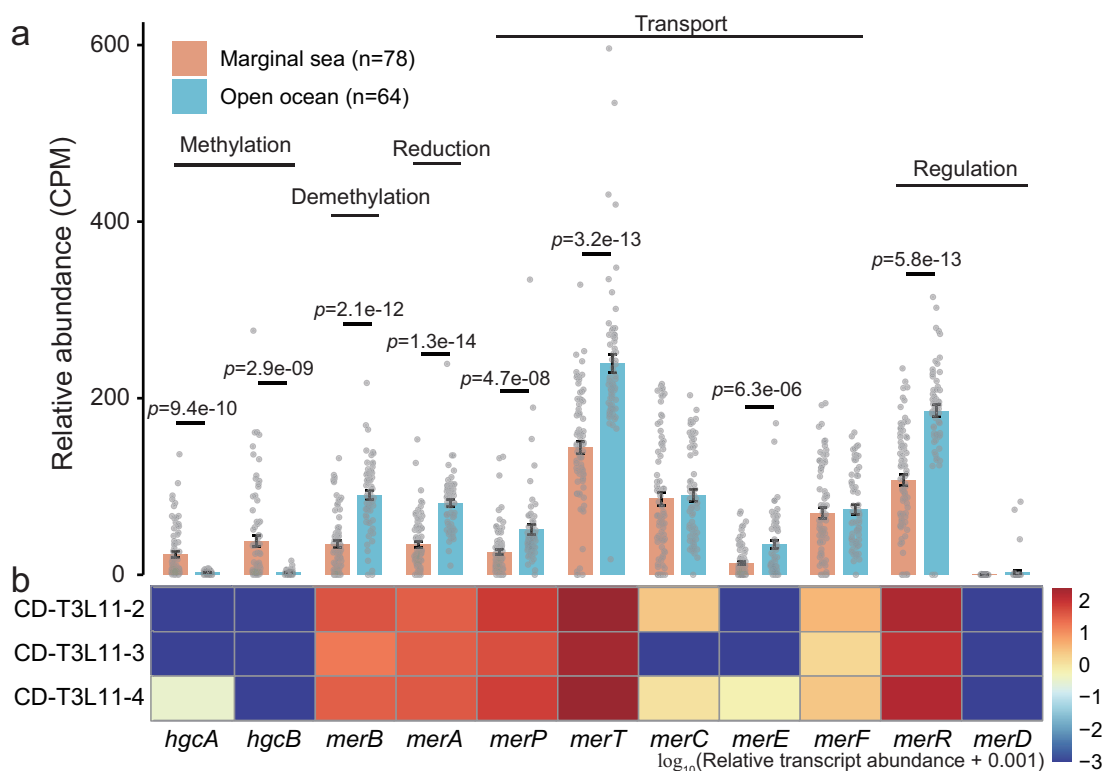


Fig. 3 | Relative abundance of mercury transforming genes in sediment metagenomes and metatranscriptomes. **a** Mean relative abundance of mercury-transforming genes extracted from MAGs in the 142 marine sediment metagenomes. The CPM values of the genes (details of genes shown in Supplementary Data 7) were calculated for the metagenomes of two groups (marginal sea and open ocean) (Supplementary Data 1 and 2). Error bars represent the standard error of the

mean. Statistical significance between the two groups was determined using the two-sided Wilcoxon test. **b** The transcripts per million (TPM) reads of metabolic genes extracted from MAGs in the three metatranscriptomes for three layers of CD-T3L11 core from Challenger Deep of the Mariana Trench. Source data are provided as a Source Data file.

metagenomic data from all samples. They were classified into 22 phyla, including 20 bacterial phyla and 2 archaeal phyla (Fig. 4a and Supplementary Data 9). The three most abundant phyla were Desulfobacterota (19), Chloroflexota (12) and Planctomycetota (10). Deltaproteobacteria-

associated *hgcA* sequences represented 59.67% of the cumulative *hgcA* abundance (quantified as CPM) across the analyzed 142 metagenomic datasets (Supplementary Fig. 7a). Since the *hgcA* genes were primarily assigned to the Deltaproteobacteria clade, we used primers specific to

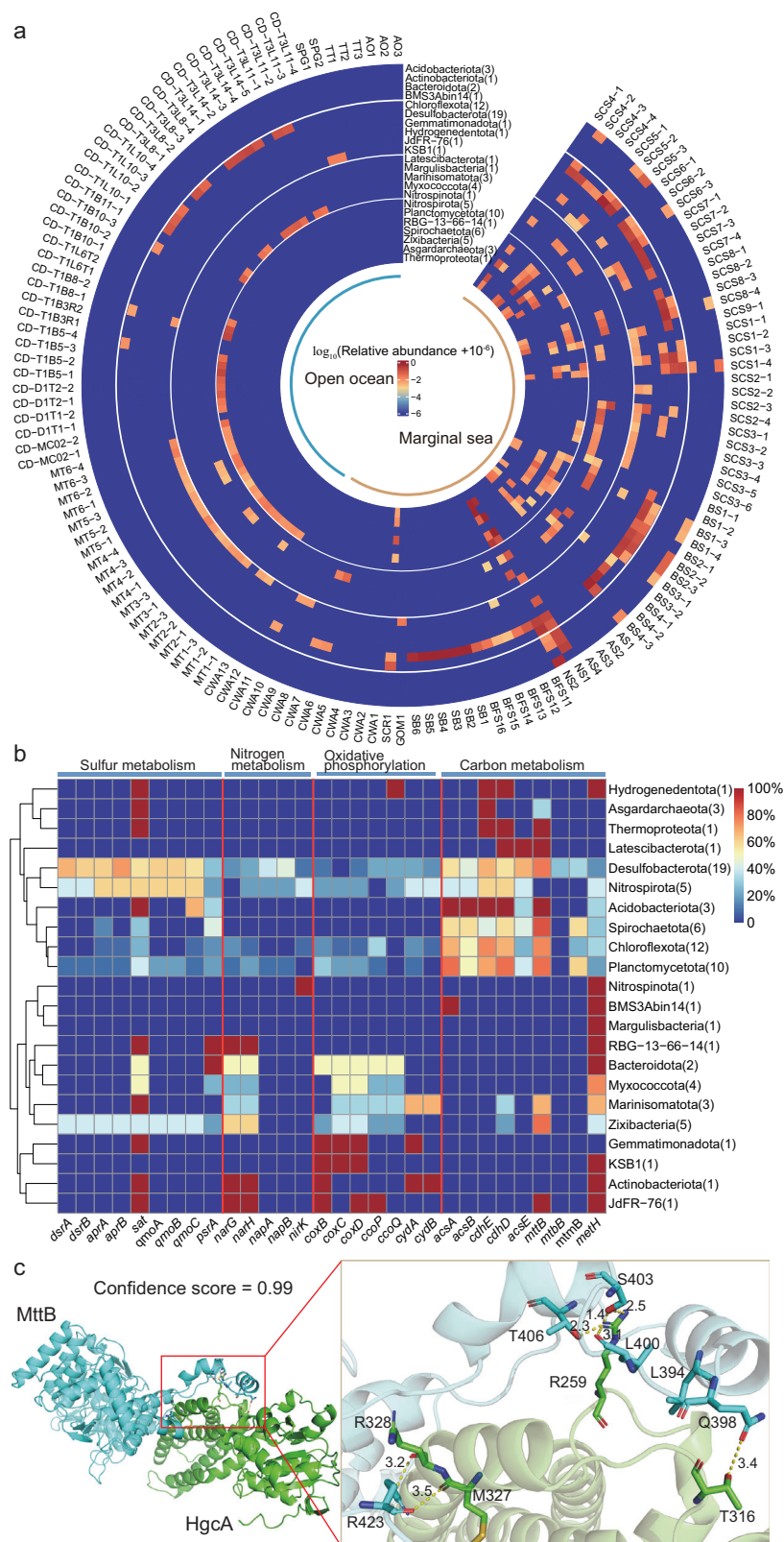


Fig. 4 | The relative abundance of Hg methylators in metagenomes and their potential functional mechanism in deep sea environments. a The relative abundance of Hg methylators in metagenomes. The MAG abundance was transformed using a logarithmic scale of 10 ($\log_{10}(\text{abundance} + 10^{-6})$). **b** Metabolic potentials of Hg methylators in the deep-sea as indicated by the functional genes

(see Supplementary Data 11 for the details of the genes). Color indicates the percentage of MAGs containing the genes. In the plot (a, b), the number of MAGs from different phyla was shown in parentheses. **c** Schematic HgcA-MttB interaction in the 3D structure. Source data are provided as a Source Data file.

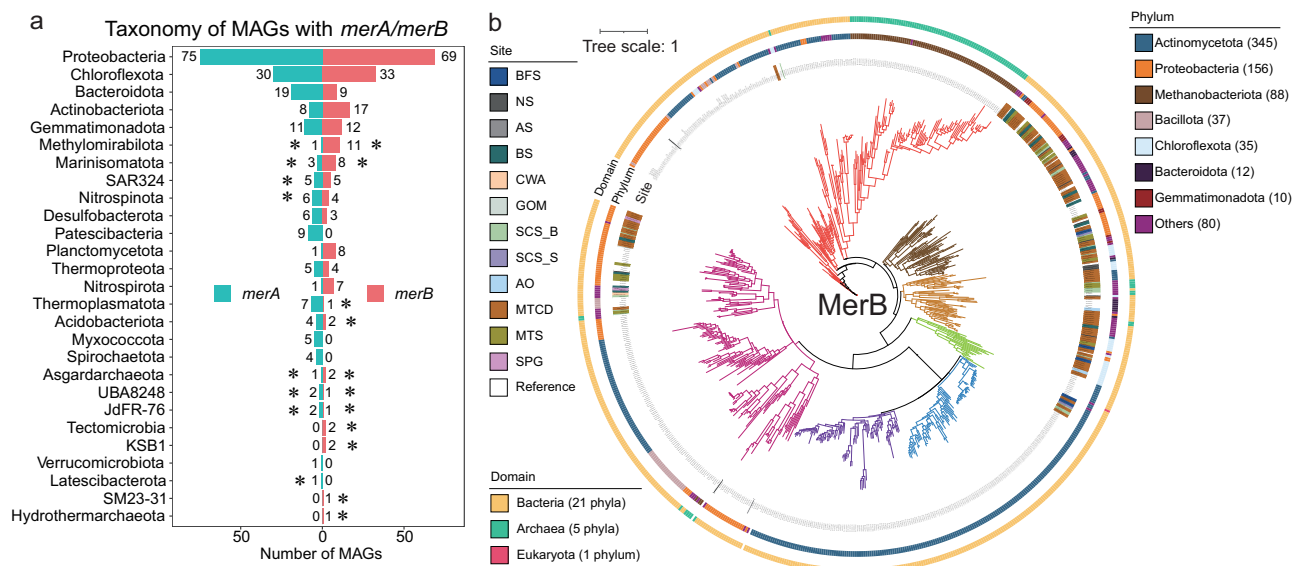


Fig. 5 | The taxonomy of newly discovered MeHg demethylating and Hg reducing microorganisms and phylogenetic tree of MerB proteins. **a** The taxonomy of newly discovered MeHg demethylating and Hg reducing microorganisms at the phylum level. The phylum with * represents the taxa of microorganisms found for the first time in this study. **b** Unrooted maximum likelihood (ML) phylogenetic tree of MerB proteins identified in the MAGs from the global marine sediments. The colors in the inner circle represent the sources of the proteins, and

those labeled as Reference were MerB proteins collected from the NCBI database. The protein number from different phyla was shown in the parentheses. *BFS* Beaufort Sea; *NS* Norwegian Sea; *AS* Arabian sea; *BS* Bashi Channel; *CWA* Coastal Western Antarctica; *GOM* Gulf of Mexico; *SCS_B* South China Sea basin; *SCS_S* South China Sea slope; *AO* Atlantic Ocean; *MTCD* Challenger Deep of Mariana Trench; *MTS* Mariana Trench slope; *SPG* South Pacific gyre U1369.

this clade to quantify their abundance with quantitative PCR assays. The results showed higher *hgcA* abundance in marginal sea samples, compared to open ocean samples (Supplementary Fig. 7b), which is in agreement with the metagenomics results. There was regional variability in the distribution of different putative MeHg producers in the sediments (Fig. 4a and Supplementary Data 10). Putative methylators from the Desulfobacterota, Spirochaetota, Zixibacteria, Asgardarchaeota, and Thermoproteota taxa were primarily found on terrestrial slopes. However, despite the fact that putative MeHg producers affiliated with Chloroflexota, KSB1, Nitrospirota, and Nitrospinota were found in the open oceans, more efforts are necessary to understand the methylation activity of these microbial methylators, as the abundance of *hgcA* in the metatranscriptomic data of the open oceans was low.

Metabolic features of Hg methylators in deep-sea sediments

To reveal the adaptability of the mercury methylators to the deep-sea environment, their metabolic potential was assessed using gene annotation (Supplementary Data 11). Genes (*dsrAB*, *aprAB*, *sat*, and *qmoABC*) involved in the sulfate reduction pathway have been identified in a number of *hgcA*-carrying MAGs, particularly in Desulfobacterota and Nitrospirota (Fig. 4b). Notably, the gene *sat* was detected in the MAGs of most taxa. Most MAGs belonging to Bacteroidota, RBG-13-66-14, and Spirochaetota harbor the gene *psrA*, which is involved in the thiosulfate reduction pathway. We also searched for marker genes, indicating the presence of the nitrate or nitrite reduction pathway in the MAGs of methylators. The genes (*narGH*) encoding nitrate reductase were found in the MAGs of 11 phyla. However, *napAB* were only found in Desulfobacterota, Nitrospirota and Planctomycetota MAGs. In addition, the gene *nirK* encoding nitrite reductase was found in Desulfobacterota, Nitrospirota, Chloroflexota and Nitrospirota MAGs. Therefore, these mercury methylators can use a variety of substances as electron acceptors. We detected some Hg methylators with some abundance in the surface layer (0–2 cm) of the sediment core (Fig. 4a), suggesting that they have a potential of oxygen

tolerance. Our functional annotation revealed that MAGs of methylators in deep-sea sediments encode a variety of terminal oxidases that may function in oxygen tolerance. Genomics analysis showed that KSB1 (GOMbin.4) contains the genes encoding the respiratory complexes cytochrome *c* oxidase (*coxBCD*), which can indicate its ability to have higher abundance in the surface layer (SCS1-1, SCS3-1, SCS5-1, MT1-1 and MT5-1) of the sediment core. Some species of Desulfobacterota and Chloroflexota include genes encoding cytochrome *c* *cbb3*-type (*ccoPQ*) oxidase. In addition, genes encoding cytochrome *bd* ubiquinol oxidase (*cydAB*) were found in the MAGs representing Desulfobacterota, Nitrospirota, Actinobacteriota, Marinisomatota and Gemmatimonadota.

To characterize the putative methyl transfer strategy in these methylators, we searched for typical cobalamin-dependent methyltransferases (Supplementary Data 12). The results showed that only cobalamin-dependent methyltransferase in Methionine synthase (MetH) or Trimethylamine metabolism (MttB, MtmB) were found among the 24 methylators (Supplementary Data 12). Of these, 14 MAGs from 11 phyla might transfer the methyl group using MetH, five MAGs from three phyla might utilize MttB to transfer the methyl group, and the remaining five MAGs might utilize both or either of the above. To verify this hypothesis, we conducted docking predictions between HgcA and MttB and between HgcA and MetH, respectively (Supplementary Data 13). Among the five MAGs utilizing MttB, the most reliable HgcA-MttB docking model had a confidence score of 0.99, and the interaction interface for this model was defined as the amino acid residues within a surface area of 3.5 Å of the encapsulated atom position (Fig. 4c and Supplementary Data 14). The docking score of −391.29 kcal/mol suggested a strong interaction between HgcA and MttB, which was mediated by 7 hydrogen bonds (Fig. 4c). The highest Arg binding activity was observed in the interaction of MttB with HgcA (Supplementary Data 14). In the hydrogen bond between Arg259 and Ser403, the closest atomic distance between MttB and HgcA was 1.4 Å (Fig. 4c).

The diversity and distribution of *merA* and *merB* carriers

There were 207 dereplicated MAGs carrying *merA* in 24 phyla (Fig. 5a and Supplementary Data 15). Among them, putative mercury reducers belonging to Nitrospinota, SAR324, Marinisomatota, UBA8248, JdFR-76, Methylomirabilota, Latescibacterota, and Asgardarchaeota were found for the first time in this research. A total of 204 dereplicated MAGs carrying *merB* were recovered, and these MAGs were distributed across 24 phyla (Fig. 5a and Supplementary Data 16). Notably, the putative methylmercury degraders affiliated with Methylomirabilota, Marinisomatota, SAR324, Thermoproteota, Nitrospinota, Acidobacteriota, Tectomicrobia, KSBI, Hydrothermarchaeota, JdFR-76, SM23-31, Thermoplasmatota, UBA8248 and Lokiarchaeota of Asgardarchaeota were reported for the first time in this study. Co-occurrence of *merA* and *merB* was revealed in 72 MAGs. Among all sediment layers, the total relative abundance of putative mercury reducers ranged from 0 to 12.05% (Supplementary Data 17), and the total relative abundance of putative methylmercury degraders ranged from 0.002% to 5.72% (Supplementary Data 18).

Phylogenetic analysis of MerB proteins

To identify deep-sea new proteins encoded by *merB* genes in all MAGs, we performed phylogenetic analysis on the inferred proteins and their known homologs in NCBI. The phylogenetic tree of MerB proteins is constituted by seven clades (Fig. 5b). The clades 2 and 3 are largely new MerB proteins, as they are composed of a low percentage of the MerB proteins existing in NCBI (20.69% and 10.96%, respectively). Among the sites investigated, a large number of *merB* sequences ($n = 97$) were retrieved from the 585 MAGs of the Challenger Deep of Mariana Trench sites with high diversity, as they were distributed in most of MerB phylogenetic clades (Fig. 5b). Aside from this, five novel MerB protein lineages were identified in the South China Sea Basin MAGs derived largely from Proteobacteria (Fig. 5b).

Discussion

Accumulation of mercury in the Western Pacific stations

This study presents an assessment of mercury concentrations within deep-sea sediments across various regions of the Western Pacific Ocean. Our findings indicate a notable gradient in total Hg levels, with sediments from the marginal slopes exhibiting significantly higher concentrations compared to those from the open ocean areas. Higher levels of mercury detected on marginal slopes might be due to increased inputs from terrestrial runoff, which carries mercury from a variety of anthropogenic and natural sources^{24,25}. An analysis of the heavy metal content in the surface sediments of the Pearl River Delta (PRD) revealed that mercury is one of the major heavy metals introduced by human activities in the surface sediments of PRD²⁶. Small particles in the marginal sea might also facilitate the precipitation of mercury compounds with terrestrial sources on to the slope sediment^{27,28}. In contrast, mercury in the open ocean sediments likely has distinct origins. Hydrothermal vents are considered a natural source of mercury, contributing to the background levels of this metal in the deep sea⁵. In addition, the deposition of mercury from the ocean surface may further augment the mercury content in these remote areas²⁰. Biogeochemical processes of mercury speciation and transport in sediments have received research attention. The different chemical forms of mercury, including its organic and inorganic species, can significantly influence its bioavailability and potential toxicity to deep-sea organisms²⁹. In marginal slope samples, deeper layers exhibited higher methylmercury content, while the opposite trend was observed in the open ocean. This is likely attributable to distinct dominant Hg-methylating microbial communities between the marginal slope and open ocean sites, which were dominated by anaerobic microorganisms (Desulfobacterota) and oxygen-tolerant types (Nitrospinota and Nitrospirota), respectively. Previous studies on methylmercury content in marine sediments have reported

concentrations of 1–40 ng/g in surface sediments of the Mediterranean Sea³⁰, while significantly lower levels (~0.21 ng/g) were detected in deep-sea cold seep sediments²¹. In our samples, methylmercury concentrations ranged from 20.30 to 65.73 ng/g. The elevated proportion of methylmercury (51.92%–91.37%) relative to total mercury in our samples might be accounted for intensified methylation processes or bioaccumulation and sedimentation dynamics within the sediment. Notably, amphipods inhabiting the Mariana Trench exhibited exceptionally high methylmercury proportions (up to 59%) of total mercury content³¹, which is close to the range of the current study.

Mercury methylators enriched on marginal slopes and their deep-sea adaptation

Mercury methylation and demethylation are pivotal processes that regulate methylmercury levels in marine ecosystems. The mechanism of Hg(II) methylation involves its accidental transport into the cytoplasm via symporters designed for essential trace metals, such as Zn(II)³². Once inside the cell, mercury is methylated and converted to MeHg, which is then expected to be excreted by an unknown efflux mechanism³³. A study based on the analysis of Hg isotopic composition in fauna and surface sediments of Mariana Trench indicates that there is little in situ production of MeHg in Mariana Trench³¹, which is in agreement with the paucity of *hgcAB* gene in the open ocean group of this study. Among anaerobic microorganisms, the methylation of inorganic Hg(II) might serve as a critical detoxification mechanism, allowing them to cope with environmental mercury exposure³⁴. It has also been suggested that the ability to produce MeHg is intrinsic and not induced by Hg exposure; however, the methylation rate of microorganisms is highly dependent on the bioavailability of mercury in the culture medium³⁵. Moreover, the potential toxicity of MeHg to the bacteria themselves still needs to be further investigated. Thus, the physiological significance of mercury methylation for microorganisms is controversial at present. In this study, the mercury methylation genes, *hgcAB*, were exclusively detected in metagenomic data from marginal sea sites, likely linked to the elevated Hg content in these environments³⁶. The abundance of *hgcAB* has been shown to be positively correlated with the total concentration of Hg³⁷.

In this study, we showed a shift in the diversity of Hg-methylated microorganisms from marginal seas to the hadal zone, which might be attributed to various ecological and environmental factors. One possibility is that the availability of mercury required for methylation might vary between marginal seas and the hadal zone. In marginal environments, the availability of anthropogenic mercury and organic matter might nourish a variety of Hg-methylating microorganisms³⁸ distinct from those in the deeper hadal zone, where the environmental conditions, such as nutrient availability and extreme pressure, could drive the selection of different inhabitants. A study indicates that dissolved organic matter (DOM) greatly inhibited Hg methylation in *Geobacter sulfurreducens* PCA but enhanced Hg methylation in *Desulfobrevibrio desulfuricans* ND132 with increasing concentrations of DOM³⁹. Another potential influencing factor is oxygen availability⁴⁰. In marginal seas, the finer sediment particle size likely results in limited oxygen penetration, leading to lower oxygen content within sediment layers. In contrast, open ocean regions with coarser sediment particles are presumed to have relatively higher oxygen levels⁴¹. Under these conditions, Desulfobacterota dominate as potential mercury-methylating microorganisms in marginal seas, while Nitrospinota and Nitrospirota emerge as key mercury methylators in open ocean environments.

At present, it is believed that biomethylation is mainly performed by sulfate-reducing bacteria (SRB), iron-reducing bacteria, and methanogens¹⁷. In this study, genes associated with sulfate reduction, particularly the *sat* gene, were detected in the majority of the MAGs, indicating that SRB are the primary Hg methylators in the deep sea. The high sulfate concentrations measured in the deep sediment by this

study might support the prevalent Hg-methylating *Desulfobacterota* bacteria. Simultaneously, the generated sulfide would react with Hg(II) to form HgS, decreasing Hg(II) biotoxicity⁴².

In previous studies, mercury methylation was reported to occur mainly in anoxic environments. Within our metagenomic data, some seemingly anaerobic Hg-methylators were found to have higher abundance in the surface oxygen-rich layers of the sediments, probably ascribed to their associated terminal oxidases. Specifically, the higher abundance of methylators affiliated with KSB1 in the surface layer of sediments likely relates to CoxBCD. A previous study revealed that CydAB-dependent KSB1 could tolerate oxygen to adapt to the bioreactor environment⁴³. Novel methylators that tolerate oxygen were identified in the Saanich Inlet characterized by the presence of an oxygen gradient⁴⁴. Similarly, Antarctic sea ice harbored the micro-aerophilic marine bacteria *Nitrospina* as a potential methylator of mercury⁴⁵. Therefore, the habitat range of the mercury methylator is much wider than previously recognized. The possible pathway of mercury methylation with genomic evidence involves the transfer of a methyl group to HgcA by a cobalamin-dependent methyltransferase, such as the CFeSP methyltransferase from the Wood-Ljungdahl pathway, CH₃-H₄MPT: CoM methyltransferase in the Wolfe cycle, 5-methyltetrahydrofolate-homocysteine methyltransferase in the methionine cycle, and methylthiol: CoM methyltransferase in the dimethylsulphoniopropionate (DMS) degradation pathway^{17,46–49}. Our study, however, identified MAGs affiliated with *Desulfobacterota*, *Spirochaetota*, and *Zixibacteria* that lacked most of the cobalamin-dependent methyltransferase genes that are generally recognized as potentially involved in mercury methylation. Instead, these MAGs contained *mttB*, encoding a trimethylamine (TMA)-specific methyltransferase, suggesting an alternative methylation mechanism. It is convenient to utilize TMA to obtain methyl in the deep-sea sediments that are probably enriched with TMA⁵⁰. This is because TMA can be produced by the degradation of a variety of precursors, including tetramethylammonium (QMA), glycine betaine, and trimethylamine oxide (TMAO), released from degrading bodies of deep-sea organisms⁵¹. QMA is often found in a variety of marine animals⁵¹. Glycine betaine and TMAO are osmolytes used by deep-sea organisms⁵². Therefore, we argue that *MttB* in these methylators might have the potential to transfer methyl from TMA to cob(I)alamin, forming methyl-cob(III)alamin, which interacts with the HgcAB complex to methylate Hg(II). The high confidence scores of the docking model of HgcA and *MttB* provide further evidence for our hypothesis. These microbial mercury methylators in the deep-sea sites probably contain specialized methylation mechanisms adapted to the characteristics of the deep-sea environment. In addition, some methylators have only one type of cobalamin-dependent methyltransferase, *MetH*, so they might utilize the methyl group in the methionine biosynthesis pathway. This methylation with the help of *MetH* has been reported in a previous study⁵³. However, these methylation mechanisms remain to be validated through microbial cultivation and isotopic tracing techniques.

Demethylator enriched in the open ocean and its novelty

In *mer*-resistant systems, the uptake of divalent inorganic Hg(II) is thought to be mediated by transporter proteins. *merT* may have multiple copies in certain microbial genomes due to its critical role as one of the important transporters in the operon^{54,55}. In addition, certain microbial strains lack *merR* in the *mer* operon⁵⁶. Thus, these two genes show different coverages in our metagenomic data. Organomercurial lyase (*MerB*) and mercury reductase (*MerA*) can demethylate MeHg to Hg(II) and subsequently reduce Hg(II) to Hg⁰ for diffusion to the extracellular space, respectively⁵⁷. We noticed that the mercury demethylation genes were detected in a considerable number of all the metagenomic data. This implies that the microorganisms in the global deep-sea sediments might rely on this process for detoxification, as the

organic mercury accumulates in the deep ocean following the food chain⁵¹. The relative abundance of *merAB* was higher in the open ocean group than in the marginal slope group, probably because the methyl group obtained by demethylation can be used for C1 metabolism to adapt to the deep-sea environment of the open ocean, where nutrient sources can be less available than soils, as organic content in these environments is variable. For methanotrophs, the methyl of methylmercury can be used as its auxiliary C1 source⁵⁸. It has been suggested that water mass age also influences *mer*-encoded prokaryotic communities in the bathypelagic deep ocean, and that the composition of DOM, particularly protein-like DOM, affects *merAB* gene expression⁵⁹. Thus, the differences of Hg cycling between sites could be related to both environmental characteristics and microbial adaptation schemes. Furthermore, the higher relative abundance of *merB* in the MAGs, compared to *merA*, implies that some microorganisms might be accompanied by an additional mechanism(s) to reduce, sequester, or redistribute the generated Hg(II)⁵⁷. The expression of *merA* and *merB* was also detected in the metatranscriptomic data. A recent study found that *merA* and *merB* were widely distributed and expressed in deep-sea waters (especially in the particle-attached fraction)⁵⁹. In addition, *merB*-mediated Hg demethylation produces Hg(II) and methane⁶⁰. Therefore, the demethylation and reduction of mercury in the waters and sediments of the global deep ocean are likely to have broader implications for the production of both methane and Hg(0) than currently understood, highlighting the need for a deeper investigation into these biogeochemical processes.

Our findings unveiled numerous previously unknown taxa capable of Hg demethylation and reduction in the deep-sea environment. The emergence of these novel Hg-transforming taxa could be linked to the horizontal gene transfer, a phenomenon known to facilitate the rapid spread of advantageous traits like mercury resistance^{15,19,61}. The *mer* operon has evolved from a simple system in geothermal environments to a widely distributed and more sophisticated detoxification system, spreading to a broader range of microbial populations through a considerable horizontal gene transfer¹⁹. Notably, our phylogenetic analysis of *MerB* indicated a complex evolutionary history, with deep-sea *MerB* sequences forming non-monophyletic lineages within the clades 2, 3 and 7 of the *MerB* phylogenetic tree, indicative of a diverse and dynamic adaptation to deep-sea habitats.

In this study, we assessed the transformative capabilities of deep-sea microbiota on mercury, utilizing metagenomes sourced from a diverse array of global marine sediments. Our results show a significant spatial heterogeneity of microbe-mediated Hg-transforming processes, with Hg methylation primarily occurring in marginal slopes and demethylation processes being more pronounced in the open ocean. The identification of Hg-methylating microbes, particularly sulfur-reducing bacteria, and their adaptation to deep-sea conditions through Hg biotransformation genes highlights the unique microbial strategies in mercury cycling. Furthermore, the discovery of novel Hg demethylation and reduction groups suggests a dynamic microbial community capable of horizontal gene transfer, potentially enhancing resistance of accumulating organic mercury in the deep ocean. These findings not only advance our understanding of mercury biogeochemistry in the deep biosphere but also have implications for bioremediation strategies and environmental monitoring of mercury pollution under different marine environments.

Methods

Sediment sampling and biogeochemical properties analyses

Eight cruises, including *R/V Tansuo01* (TS01, June–August of 2016), *R/V Tansuo03* (TS03, January–March of 2017), *R/V Tansuo07* (TS07, April–May of 2018), *R/V Tansuo12* (TS12, June–July of 2019), *R/V Tansuo14* (TS14, September–October of 2019), *R/V Tansuo16* (TS16, March of 2020), *R/V Dayang 37-II* (DY37II, June–July of 2016), and *R/V HaiXing6000* (HXROV, October of 2018), yielded a total of 32 sediment

cores from South China Sea, Bashi Channel, northern slope of the Mariana Trench, and Challenger Deep of Mariana Trench at depths ranging from 1087 to 10,909 m (Fig. 1a, b and Supplementary Data 1). Upon arriving on board, all of the intact core samples were cut into 2- or 3-cm layers at room temperature and then frozen at -80°C until needed. The layers used in the metatranscriptomics study were preserved using RNALater (TaKaRa, Dalian, China).

To extract the pore water from the sediment samples, they were centrifuged at $2000\times g$ for 15 min. The pore water was next filtered through $0.22\text{ }\mu\text{m}$ pore-size cellulose acetate membranes to measure environmental parameters. An automated continuous-flow SEAL AA500 analyzer spectrophotometer (SEAL Analytical, Norderstedt, Germany) was used to measure the concentrations of ammonium (NH_4^+), nitrate (NO_3^-), nitrite (NO_2^-), and soluble reactive phosphate (PO_4^{3-}) in the sediment pore water. Sulfate and iron concentrations in the pore water were measured using a Dionex ion chromatography system (Aquion IC, Thermo Fisher Scientific, USA) and inductively coupled plasma-optical emission spectroscopy (Spectro Arcos, Spectro, Germany), respectively. A Vario Micro Cube elemental analyzer (Elementar, Langenselbold, Germany) was used to measure the concentrations of total nitrogen (TN) and total organic carbon (TOC) in the sediments. Total mercury was analyzed according to the Chinese standard (HJ680-2013). A 0.5-g ($\pm 0.0001\text{ g}$) homogenized sample was mixed with 6 ml of 12 M hydrochloric acid (Guangzhou Chemical Reagent Factory, Guangzhou, China cat#CB11-TD) and 2 ml of 16 M nitric acid (Guangzhou Chemical Reagent Factory, Guangzhou, China cat#CD18). The mixed solution was heated at 150°C for 5 min to digest the sample. The total mercury was estimated with atomic fluorescence spectrometry (BAF-2000, Baode, China; HPLC, BSA-100, Baode, China). The recovery rate of the marine sediment standard sample GBW07316 was 98.31%. Approximately 0.2 g of sediment samples were processed via ultrasonication-assisted hydrochloric acid extraction for mercury speciation analysis⁶², followed by quantification of methylmercury and Hg(II) using high-performance liquid chromatography coupled with atomic fluorescence spectrometry (ELSP-2, Prin-Cen, China).

Nucleic acids extraction, library preparation, and quantitative PCR

The PowerMax soil DNA isolation kit (MoBio, Carlsbad, CA, USA cat#12988-10) was used to extract DNA from at least a 10-g sediment sample, according to the manufacturer's instructions. The Qubit dsDNA HS Assay Kit (Thermo Fisher Scientific, USA cat#Q32854) and a Qubit 2.0 fluorometer (Invitrogen, Carlsbad, CA, USA) were used to measure the concentration of DNA. Prior to library preparation, DNA samples containing $\leq 2\text{ ng}/\mu\text{L}$ were concentrated using AMPure XP beads (Beckman Colter, CA cat#A63881). Using a TruSeq Nano DNA LT Library Preparation Kit (Illumina, California, USA cat#FC-121-4002), 100 ng of genomic DNA was used to create libraries with insert sizes of 350 bp or 550 bp. The same protocol for DNA extraction was applied to two blank control samples as controls.

RNA extraction was performed on three layers (6–9, 12–15, and 18–21 cmbsf) of sediment sample T3L11 from Challenger Deep of Mariana Trench (Supplementary Data 1). Using a PowerSoil Total RNA Isolation Kit (MoBio, Carlsbad, CA, USA cat#12866-25) and following the manufacturer's instructions, total RNA was extracted from the sediment layers. We extracted RNA in duplicate from each sample. The pooled RNA was enriched using a single RNA-binding column, and the results were measured using a Qubit 4.0 Fluorometer (Invitrogen, Carlsbad, CA, USA). As directed by the manufacturer, the RNA extracts were treated with TURBO DNase (Invitrogen, Waltham, MA, USA cat#AM2238) to ensure DNA deletion. To confirm that all DNA was removed, about 1 ng of the resulting RNA was used as a template for PCR using a pair of broad-range 16S rRNA gene-specific primers, 341F (5'-

CCTAYGGGRBGCASCAG-3') and 802R (5'-TACNVGGGTATCTA ATCC-3'). The remaining RNA was transformed into cDNA (ds-cDNA) with the help of the Ovation® RNA-Seq System V2 kit (NuGEN, San Carlos, CA, USA cat#7102). The TruePrep DNA Library Prep Kit for Illumina V2 (Vazyme, Jiangsu, China cat#TD503) was utilized to create metatranscriptome libraries with an insert size of 150 bp utilizing a total of 100 ng of cDNA.

Quantitative PCR analysis was performed in triplicate using a LightCycler 480 II real-time PCR system (Roche, Rotkreuz, Switzerland) to quantify representative DNA samples (Supplementary Fig. 7b). Primer specific to the *hgcA* gene of the Deltaproteobacteria clade were employed (ORNL-Delta-HgcA-F: 5'-GCCAACTACA AGMTGASCTWC-3'; ORNL-Delta-HgcA-R: 5'-CCSGCNGCACCACGACRTT-3'), as this group represents the predominant *hgcA*-harboring taxa in the sediments (Supplementary Fig. 7a). Thermal cycling reaction was performed with the following conditions and duration: an initial denaturation at 95°C for 3 min, followed by 35 cycles of 95°C for 30 s, 57°C for 30 s, and 72°C for 30 s. An external standard curve ($R^2=0.999$) spanning 2.96×10^2 to 2.96×10^7 copies/ μL was generated by serial 10-fold dilutions of a plasmid containing the target *hgcA* fragment (cloned using the pMD™18-T Vector Cloning Kit, Takara cat# 6011).

"Omics" data sequencing and quality control

The Illumina Miseq $2\times 300\text{ bp}$, Illumina Hiseq 2×150 or Illumina Novaseq $6000\text{ }2\times 150\text{ bp}$ platforms were used to sequence the DNA/cDNA libraries (Supplementary Data 1). After adapters were removed from the raw sequencing reads, fastp (v.0.20.0) was used to filter the data with the parameters (-w 16 -q 20 -u 20 -g -c -W 5 -3 -I 50)⁶³. FastUniq (v1.1) was used with the default parameters to eliminate duplicate paired-end reads⁶⁴. Reads that Bowtie2 (v.2.4.1) mapped to two control metagenomes were eliminated⁶⁵. Metagenomic data from a worldwide collection of sediment samples were sourced from the NCBI (Supplementary Data 2). The reference marine sediment metagenomic data were assembled using the same metagenomics method.

Microbial novelty and diversity analyses

Ribosomal RNA gene fragments (5S, 16S, and 23S) were detected with rna_hmm3.py from qualified metagenomic reads (miTags)⁶⁶. The V4 hypervariable regions of 16S rRNA genes (16S miTags) were isolated using a custom script (https://github.com/heyinghui22/mitag_analysis/blob/main/mitag_analysis-command/running16S.sh) and subsequently analyzed on the Qiime2 platform with the Classify-consensus-vsearch command to classify the representative miTags⁶⁷. ACE, Chao1 and Shannon indices were calculated on the Qiime2 platform as well. The 16S miTag sequences were scanned by BLASTn (v.2.9.0) against the SILVA 138 SSU database, and novel 16S miTags were identified at the species level using 97% similarity as a threshold. The ratio of novel 16S miTags was calculated by dividing the number of novel 16S miTags recognized in each sample by the total number of 16S miTags contained in each sample. The MNS⁶⁸ was calculated by importing the classification and abundance results obtained from Parallel-META 3⁶⁹ into the microbiome search engine web tool (<http://mse.single-cell.cn/index.php/mse>). We used the ribosomal protein S3 gene (*rpS3*) sequences to assess community structural differences across different sites. The *rpS3* sequences were identified by searching all predicted proteins from the assemblies using HMMER3 with a custom hidden Markov model, applying a score threshold of 40⁷⁰. Only *rpS3* proteins with amino acid lengths exceeding 180 residues were retained⁷¹. These sequences were clustered at 99% identity using USEARCH (-sort length -id 0.99 -maxrejects 0 -maxaccepts 0) to generate species-level groups, termed species groups (SGs). To quantify SG abundances, the reads from each sample were mapped to the longest *rpS3*-containing contig within each cluster using Bowtie2. Mapped reads were filtered with CoverM v0.6.1 (filter --min-read-

percent-identity 99 --min-read-aligned-percent 75)⁷². The coverage of each contig was calculated using the “mean” method in CoverM v0.6.1. The relative abundance of each SG in a sample was computed as its coverage divided by the total coverage of all contigs. The resulting Bray-Curtis dissimilarity matrix based on the relative abundance served as input for downstream PCoA analyses to assess the overall dissimilarity level of the prokaryotic community structures of the different sites. The relationship between prokaryotic communities at selected study sites and their corresponding environmental factors, including nitrate, nitrite, ammonia, phosphate, TOC and TN, was analyzed using CCA⁷³.

Assembly, genome binning and abundance calculation

To achieve better assembly results, high-quality reads of sediment layers from the same core were merged for a co-assembly using Megahit (v1.2.8) using a kmer range of 21 to 141 and a k-step of 10 (-min contig len 300 m 0.9 k min 21 -k-max 141-k-step 10). The Bining module of MetaWRAP v 1.2.1 (-maxbin2 -concoction -metabat2) was used to recover MAGs from the contigs longer than 2 kb⁷⁴. The reads from the individual metagenomes were mapped on the selected contigs to calculate coverage level and tetranucleotide frequencies for subsequent MAG binning for a sediment core. The refinement of the MAGs was performed with the bin_refinement module of MetaWRAP (-c 50 -x 10). MAGs were examined and filtered with low integrity (<50%) and high contamination (>10%) by CheckM (v1.0.11)⁷⁵. To remove redundant MAGs, the most representative genomes were chosen using dRep (v1.4.3) based on a 99% average nucleotide identity (ANI) cutoff⁷⁶. Using GTDB-tk⁷⁷ combined with the GTDB release 207, the genomes were taxonomically classified. The relative abundance of MAGs was calculated using the relative_abundance method of CoverM (v.0.4.0, with the settings -min-read-aligned-length 50 min-read-percent-identity 0.99 min-covered-fraction 0.1 --proper-pairs-only in genome mode) (<https://github.com/wwood/CoverM>). The workflow diagram for the metagenomic analysis was shown in Supplementary Fig. 8.

Metagenomic annotation and assessment of gene abundance

Prodigal (v2.6.2)⁷⁸ was used to predict coding sequences and encoded proteins from MAGs and assembled contigs, respectively. KofamScan⁷⁹ was used to annotate proteins against the KEGG Ortholog database. The retrieved MerA and MerB sequences were manually screened for conserved catalytic residues: cysteine pair (Cys207/Cys212, *Bacillus sp.* RC607 numbering) of MerA⁸⁰ and Cys96, Cys159, and Asp99 (plasmid R831 MerB numbering) of MerB⁸¹. To further collect *hgcA* and *hgcB*, all predicted protein sequences in the metagenomes were used to search against the amino acid sequences of HgcAB in the Hg MATE database⁸² using hmmsearch with E-value ≤ 1e-05 as the cutoff. Each hit was then manually confirmed by verifying the presence of the conserved sequence structural domains (HgcA: cap-helix structural domain (N(V/I)WCA(A/G)); HgcB: CX2CX2CX3C, respectively)¹⁷. The taxonomic origin of functional gene sequences was predicted based on the GTDB taxonomy of the MAGs that contain the functional genes in the phylogenetic tree. The abundance of functional genes was calculated using Salmon software (v1.10.2) in metagenome mode⁸³.

HgcA-MttB protein interaction simulation and analysis

The three-dimensional protein structures of HgcA and MttB were predicted using ColabFold⁸⁴. The binding conformation between HgcA and MttB was predicted using the HDock server (<http://hdock.phys.hust.edu.cn/>)⁸⁵. Higher confidence scores above 0.70 suggest a higher likelihood of a molecule attaching to another. A possible binding contact between two molecules is indicated by confidence scores between 0.50 and 0.70. A low likelihood of binding between two protein molecules is indicated by a confidence score of less than 0.50.

The docking structures of the two proteins were visualized in PyMOL (v2.1.0).

Phylogenetics analysis

Reference proteins encoded by *merB* that have been published were downloaded from the NCBI database. For the construction of the MerB phylogenetic tree, CD-HIT (v4.8.1) used 95% similarity thresholds to remove redundant sequences⁸⁶. MAFFT (v7.505) was used for the alignment of the remaining sequences⁸⁷. The maximum likelihood (ML) tree was rebuilt using IQ-TREE v1.6⁸⁸ using the WAG + F + I + R9 protein substitution model, which was chosen based on the Bayesian Information Criterion (BIC), after the alignment had been trimmed using trimAl v1.2⁸⁹. The phylogenetic tree was visualized using the Interactive Tree of Life (iTOL v.4).

Reporting summary

Further information on research design is available in the Nature Portfolio Reporting Summary linked to this article.

Data availability

The assembled Contig and MAG sequences data generated in this study have been deposited in the NCBI database under the accession codes PRJNA635214 [<https://www.ncbi.nlm.nih.gov/bioproject/635214>] and PRJNA1051299 [<https://www.ncbi.nlm.nih.gov/bioproject/1051299>]. The raw sequencing data used in this study are available in the NCBI database under accession codes PRJNA524407, PRJNA573088, PRJNA380945, PRJNA504765, PRJEB25358, PRJNA264715, PRJNA309469, PRJNA297058, PRJNA340165, PRJNA341273. Source data are provided in this paper.

Code availability

The custom scripts used in this study are publicly available at GitHub (https://github.com/ZhuoboLi/Mercury_metagenomics) and in Zenodo <https://doi.org/10.5281/zenodo.16269052>. (<https://zenodo.org/records/16269052>).

References

- Bowman, K. L., Lamborg, C. H. & Agather, A. M. A global perspective on mercury cycling in the ocean. *Sci. Total Environ.* **710**, 136166 (2020).
- Mason, R. P. et al. The air-sea exchange of mercury in the low latitude Pacific and Atlantic Oceans. *Deep Sea Res. I Oceanogr. Res. Pap.* **122**, 17–28 (2017).
- Amos, H. M. et al. Global biogeochemical implications of mercury discharges from rivers and sediment burial. *Environ. Sci. Technol.* **48**, 9514–9522 (2014).
- Ganguli, P. M., Conaway, C. H., Swarzenski, P. W., Izbicki, J. A. & Flegal, A. R. Mercury speciation and transport via submarine groundwater discharge at a Southern California coastal lagoon system. *Environ. Sci. Technol.* **46**, 1480–1488 (2012).
- Torres-Rodriguez, N. et al. Mercury fluxes from hydrothermal venting at mid-ocean ridges constrained by measurements. *Nat. Geosci.* **17**, 51–57 (2024).
- Liu, M. et al. Rivers as the largest source of mercury to coastal oceans worldwide. *Nat. Geosci.* **14**, 672–677 (2021).
- Meng, M. et al. Distribution of mercury in coastal marine sediments of China: Sources and transport. *Mar. Pollut. Bull.* **88**, 347–353 (2014).
- Fitzgerald, W. F., Lamborg, C. H. & Hammerschmidt, C. R. Marine biogeochemical cycling of mercury. *Chem. Rev.* **107**, 641–662 (2007).
- Fitzgerald, W. F. & Clarkson, T. W. Mercury and monomethylmercury: present future concerns. *Environ. Health Perspect.* **96**, 159–166 (1991).

10. Selin, N. E. Global biogeochemical cycling of mercury: A review. *Annu. Rev. Env. Resour.* **34**, 43–63 (2009).
11. Hsu-Kim, H., Eckley, C. S. & Selin, N. E. Modern science of a legacy problem: mercury biogeochemical research after the Minamata Convention. *Environ. Sci. Process. Impacts* **20**, 582–583 (2018).
12. Lee, C.-S. & Fisher, N. S. Bioaccumulation of methylmercury in a marine copepod. *Environ. Toxicol. Chem.* **36**, 1287–1293 (2017).
13. Chetelat, J., Ackerman, J. T., Eagles-Smith, C. A. & Hebert, C. E. Methylmercury exposure in wildlife: A review of the ecological and physiological processes affecting contaminant concentrations and their interpretation. *Sci. Total Environ.* **711**, 135117 (2020).
14. Feng, L., Li, P. & Feng, X. Methylmercury bioaccumulation in rice and health effects: A systematic review. *Curr. Opin. Environ. Sci. Health* **23**, 100285 (2021).
15. Christakis, C. A., Barkay, T. & Boyd, E. S. Expanded diversity and phylogeny of *mer* genes broadens mercury resistance paradigms and reveals an origin for MerA among thermophilic archaea. *Front. Microbiol.* **12**, 682605 (2021).
16. McDaniel, E. A. et al. Expanded phylogenetic diversity and metabolic flexibility of mercury-methylating microorganisms. *mSystems* **5**, e00299–00220 (2020).
17. Parks, J. M. et al. The genetic basis for bacterial mercury methylation. *Science* **339**, 1332–1335 (2013).
18. Ma, M., Du, H. & Wang, D. Mercury methylation by anaerobic microorganisms: A review. *Crit. Rev. Environ. Sci. Technol.* **49**, 1893–1936 (2019).
19. Barkay, T., Miller, S. M. & Summers, A. O. Bacterial mercury resistance from atoms to ecosystems. *FEMS Microbiol. Rev.* **27**, 355–384 (2003).
20. Blum, J. D. et al. Mercury isotopes identify near-surface marine mercury in deep-sea trench biota. *Proc. Natl. Acad. Sci. USA* **117**, 29292–29298 (2020).
21. Li, J. et al. Deep sea cold seeps are a sink for mercury and source for methylmercury. *Commun. Earth Environ.* **5**, 324 (2024).
22. Zhou, Y.-L., Mara, P., Cui, G.-J., Edgcomb, V. P. & Wang, Y. Microbiomes in the Challenger Deep slope and bottom-axis sediments. *Nat. Commun.* **13**, 1515 (2022).
23. Li, W.-L. et al. Microbial ecology of sulfur cycling near the sulfate-methane transition of deep-sea cold seep sediments. *Environ. Microbiol.* **23**, 6844–6858 (2021).
24. Yu, C. et al. Transport of mercury in a regulated high-sediment river and its input to marginal seas. *Water Res.* **214**, 118211 (2022).
25. Yin, R. et al. Mercury inputs to Chinese marginal seas: Impact of industrialization and development of China. *J. Geophys. Res. Oceans* **123**, 5599–5611 (2018).
26. Zhao, G., Ye, S., Yuan, H., Ding, X. & Wang, J. Surface sediment properties and heavy metal pollution assessment in the Pearl River Estuary, China. *Environ. Sci. Pollut. Res.* **24**, 2966–2979 (2017).
27. Zhang, Y. et al. Biogeochemical drivers of the fate of riverine mercury discharged to the global and Arctic oceans. *Glob. Biogeochem. Cycles* **29**, 854–864 (2015).
28. Kim, J. et al. Sedimentary mercury (Hg) in the marginal seas adjacent to Chinese high-Hg emissions: Source-to-sink, mass inventory, and accumulation history. *Mar. Pollut. Bull.* **128**, 428–437 (2018).
29. Cruz-Acevedo, E. et al. Mercury bioaccumulation patterns in deep-sea fishes as indicators of pollution scenarios in the northern Pacific of Mexico. *Deep Sea Res. I Oceanogr. Res. Pap.* **144**, 52–62 (2019).
30. Spada, L., Annicchiarico, C., Cardellicchio, N., Giandomenico, S. & Di Leo, A. Mercury and methylmercury concentrations in Mediterranean seafood and surface sediments, intake evaluation and risk for consumers. *Int. J. Hyg. Environ. Health* **215**, 418–426 (2012).
31. Sun, R. et al. Methylmercury produced in upper oceans accumulates in deep Mariana Trench fauna. *Nat. Commun.* **11**, 3389 (2020).
32. Schaefer, J. K., Szczuka, A. & Morel, F. M. M. Effect of divalent metals on Hg(II) uptake and methylation by bacteria. *Environ. Sci. Technol.* **48**, 3007–3013 (2014).
33. Luo, H. et al. Recent advances in microbial mercury methylation: A review on methylation habitat, methylator, mechanism, and influencing factor. *Process Saf. Environ. Prot.* **170**, 286–296 (2023).
34. Schaefer, J. K. et al. Active transport, substrate specificity, and methylation of Hg(II) in anaerobic bacteria. *Proc. Natl. Acad. Sci. USA* **108**, 8714–8719 (2011).
35. Gilmour, C. C. et al. Sulfate-reducing bacterium *Desulfovibrio desulfuricans* ND132 as a model for understanding bacterial mercury methylation. *Appl. Environ. Microbiol.* **77**, 3938–3951 (2011).
36. Capo, E. et al. Expression levels of *hgcAB* genes and mercury availability jointly explain methylmercury formation in stratified brackish waters. *Environ. Sci. Technol.* **56**, 13119–13130 (2022).
37. Zhang, R. et al. Mining-impacted rice paddies select for Archaeal methylators and reveal a putative (Archaeal) regulator of mercury methylation. *ISME Commun.* **3**, 74 (2023).
38. Wang, Y.-L., Ikuma, K., Brown, A. M. V. & Deonaraine, A. Global survey of *hgcA*-carrying genomes in marine and freshwater sediments: Insights into mercury methylation processes. *Environ. Pollut.* **352**, 124117 (2024).
39. Zhao, L. et al. Contrasting effects of dissolved organic matter on mercury methylation by *Geobacter sulfurreducens* PCA and *Desulfovibrio desulfuricans*. *Environ. Sci. Technol.* **51**, 10468–10475 (2017). ND132.
40. Cabrol, L. et al. Redox gradient shapes the abundance and diversity of mercury-methylating microorganisms along the water column of the Black Sea. *mSystems* **8**, e00537–00523 (2023).
41. Li, Z., He, Y., Zhang, H., Qian, H. & Wang, Y. Biotransformations of arsenic in marine sediments across marginal slope to hadal zone. *J. Hazard Mater.* **480**, 135955 (2024).
42. Liu, J. et al. Understanding of mercury and methylmercury transformation in sludge composting by metagenomic analysis. *Water Res.* **226**, 119204 (2022).
43. Li, Q., Zhou, Y., Lu, R., Zheng, P. & Wang, Y. Phylogeny, distribution and potential metabolism of candidate bacterial phylum KSB1. *PeerJ* **10**, e13241 (2022).
44. Lin, H. et al. Mercury methylation by metabolically versatile and cosmopolitan marine bacteria. *ISME J.* **15**, 1810–1825 (2021).
45. Gionfriddo, C. M. et al. Microbial mercury methylation in Antarctic sea ice. *Nat. Microbiol.* **1**, 16127 (2016).
46. Doukov, T., Seravalli, J., Stezowski, J. J. & Ragsdale, S. V. Crystal structure of a methyltetrahydrofolate- and corrinoid-dependent methyltransferase. *Structure* **8**, 817–830 (2000).
47. Gao, J. et al. The origin of methyl group in methanogen-mediated mercury methylation: From the Wolfe cycle. *Proc. Natl. Acad. Sci. USA* **121**, e2416761121 (2024).
48. Landner, L. Biochemical model for the biological methylation of mercury suggested from methylation studies in vivo with *Neurospora crassa*. *Nature* **230**, 452–454 (1971).
49. Larose, C. et al. Springtime changes in snow chemistry lead to new insights into mercury methylation in the Arctic. *Geochim. Cosmochim. Acta* **74**, 6263–6275 (2010).
50. Zhuang, G.-C. et al. Distribution and isotopic composition of trimethylamine, dimethylsulfide and dimethylsulfoniopropionate in marine sediments. *Mar. Chem.* **196**, 35–46 (2017).
51. Bueno de Mesquita, C. P., Wu, D. & Tringe, S. G. Methyl-based methanogenesis: An ecological and genomic review. *Microbiol. Mol. Biol. Rev.* **87**, e00024–00022 (2023).
52. Downing, A. B., Wallace, G. T. & Yancey, P. H. Organic osmolytes of amphipods from littoral to hadal zones: Increases with depth in trimethylamine N-oxide, scyllo-inositol and other potential pressure counteractants. *Deep Sea Res. I Oceanogr. Res. Pap.* **138**, 1–10 (2018).
53. Liu, S. et al. Phylogenetic and ecophysiological novelty of subsurface mercury methylators in mangrove sediments. *ISME J.* **17**, 2313–2325 (2023).

54. Hamlett, N. V., Landale, E. C., Davis, B. H. & Summers, A. O. Roles of the Tn21 merT, merP, and merC gene products in mercury resistance and mercury binding. *J. Bacteriol.* **174**, 6377–6385 (1992).
55. Zhang, J., Zeng, Y., Liu, B. & Deng, X. MerP/MerT-mediated mechanism: A different approach to mercury resistance and bioaccumulation by marine bacteria. *J. Hazard Mater.* **388**, 122062 (2020).
56. Moller, A. K. et al. Mercuric reductase genes (*merA*) and mercury resistance plasmids in High Arctic snow, freshwater and sea-ice brine. *FEMS Microbiol. Ecol.* **87**, 52–63 (2014).
57. Krout, I. N., Scrimale, T., Vorojeikina, D., Boyd, E. S. & Rand, M. D. Organomercurial lyase (MerB)-mediated demethylation decreases bacterial methylmercury resistance in the absence of mercuric reductase (MerA). *Appl. Environ. Microbiol.* **88**, e00010–e00022 (2022).
58. Lu, X. et al. Methylmercury uptake and degradation by methanotrophs. *Sci. Adv.* **3**, 1700041 (2017).
59. Sanz-Saez, I. et al. Microorganisms involved in methylmercury demethylation and mercury reduction are widely distributed and active in the bathypelagic deep ocean waters. *Environ. Sci. Technol.* **58**, 13795–13807 (2024).
60. Schaefer, J. K. et al. Role of the bacterial organomercury lyase (MerB) in controlling methylmercury accumulation in mercury-contaminated natural waters. *Environ. Sci. Technol.* **38**, 4304–4311 (2004).
61. Zheng, J. et al. Diverse methylmercury (MeHg) producers and degraders inhabit acid mine drainage sediments, but few taxa correlate with MeHg accumulation. *mSystems* **8**, e00736–00722 (2023).
62. Shang, X., Zhao, Y., Zhang, L., Li, X. & Wu, Y. Improvement of the method for methylmercury determination in aquatic products using liquid chromatography online coupled with atomic fluorescence spectrometry. *Chin. J. Chromatogr.* **29**, 667–672 (2011).
63. Chen, S., Zhou, Y., Chen, Y. & Gu, J. fastp: an ultra-fast all-in-one FASTQ preprocessor. *Bioinformatics* **34**, 884–890 (2018).
64. Xu, H. et al. FastUniq: A fast de novo duplicates removal tool for paired short reads. *PLoS ONE* **7**, e52249 (2012).
65. Langmead, B. & Salzberg, S. L. Fast gapped-read alignment with Bowtie 2. *Nat. Methods* **9**, 357–359 (2012).
66. Huang, Y., Gilna, P. & Li, W. Identification of ribosomal RNA genes in metagenomic fragments. *Bioinformatics* **25**, 1338–1340 (2009).
67. Bolyen, E. et al. Reproducible, interactive, scalable and extensible microbiome data science using QIIME 2. *Nat. Biotechnol.* **37**, 852–857 (2019).
68. Su, X. et al. Identifying and predicting novelty in microbiome studies. *mBio* **9**, e02099–02018 (2018).
69. Jing, G. et al. Parallel-META 3: Comprehensive taxonomical and functional analysis platform for efficient comparison of microbial communities. *Sci. Rep.* **7**, 40371 (2017).
70. Diamond, S. et al. Mediterranean grassland soil C-N compound turnover is dependent on rainfall and depth, and is mediated by genomically divergent microorganisms. *Nat. Microbiol.* **4**, 1356–1367 (2019).
71. Voutsinos, M. Y., West-Roberts, J. A., Sachdeva, R., Moreau, J. W. & Banfield, J. F. Weathered granites and soils harbour microbes with lanthanide-dependent methylotrophic enzymes. *BMC Biol.* **22**, 41 (2024).
72. Zhang, D. et al. Microbe-driven elemental cycling enables microbial adaptation to deep-sea ferromanganese nodule sediment fields. *Microbiome* **11**, 160 (2023).
73. Terbraak, C. J. F. Canonical correspondence analysis: a new eigenvector technique for multivariate direct gradient analysis. *Ecology* **67**, 1167–1179 (1986).
74. Uritskiy, G. V., DiRuggiero, J. & Taylor, J. MetaWRAP—a flexible pipeline for genome-resolved metagenomic data analysis. *Microbiome* **6**, 158 (2018).
75. Parks, D. H., Imelfort, M., Skennerton, C. T., Hugenholtz, P. & Tyson, G. W. CheckM: assessing the quality of microbial genomes recovered from isolates, single cells, and metagenomes. *Genome Res.* **25**, 1043–1055 (2015).
76. Olm, M. R., Brown, C. T., Brooks, B. & Banfield, J. F. dRep: a tool for fast and accurate genomic comparisons that enables improved genome recovery from metagenomes through de-replication. *ISME J.* **11**, 2864–2868 (2017).
77. Chaumeil, P.-A., Mussig, A. J., Hugenholtz, P. & Parks, D. H. GTDB-Tk: a toolkit to classify genomes with the Genome Taxonomy Database. *Bioinformatics* **36**, 1925–1927 (2020).
78. Hyatt, D. et al. Prodigal: prokaryotic gene recognition and translation initiation site identification. *BMC Bioinform.* **11**, 119 (2010).
79. Aramaki, T. et al. KofamKOALA: KEGG Ortholog assignment based on profile HMM and adaptive score threshold. *Bioinformatics* **36**, 2251–2252 (2020).
80. Boyd, E. S. & Barkay, T. The mercury resistance operon: from an origin in a geothermal environment to an efficient detoxification machine. *Front. Microbiol.* **3**, 349 (2012).
81. Pitts, K. E. & Summers, A. O. The roles of thiols in the bacterial organomercurial lyase (MerB). *Biochemistry* **41**, 10287–10296 (2002).
82. Capo, E. et al. A consensus protocol for the recovery of mercury methylation genes from metagenomes. *Mol. Ecol. Resour.* **23**, 190–204 (2023).
83. Patro, R., Duggal, G., Love, M. I., Irizarry, R. A. & Kingsford, C. Salmon provides fast and bias-aware quantification of transcript expression. *Nat. Methods* **14**, 417–419 (2017).
84. Mirdita, M. et al. ColabFold: making protein folding accessible to all. *Nat. Methods* **19**, 679–682 (2022).
85. Yan, Y., Tao, H., He, J. & Huang, S.-Y. The HDock server for integrated protein-protein docking. *Nat. Protoc.* **15**, 1829–1852 (2020).
86. Li, W. & Godzik, A. Cd-hit: a fast program for clustering and comparing large sets of protein or nucleotide sequences. *Bioinformatics* **22**, 1658–1659 (2006).
87. Katoh, K. & Standley, D. M. MAFFT multiple sequence alignment software version 7: improvements in performance and usability. *Mol. Biol. Evol.* **30**, 772–780 (2013).
88. Lam-Tung, N., Schmidt, H. A., von Haeseler, A. & Bui Quang, M. IQ-TREE: a fast and effective stochastic algorithm for estimating maximum-likelihood phylogenies. *Mol. Biol. Evol.* **32**, 268–274 (2015).
89. Capella-Gutierrez, S., Silla-Martinez, J. M. & Gabaldon, T. trimAl: a tool for automated alignment trimming in large-scale phylogenetic analyses. *Bioinformatics* **25**, 1972–1973 (2009).

Acknowledgements

This work is supported by the National Natural Science Foundation of China (42376149) (Y.W.) and Shenzhen Key Laboratory of Advanced Technology for Marine Ecology (ZDSYS20230626091459009) (Y.W.). We thank crew members of R/V Tansuo Yihao and Tansuo Erhao for the sampling work.

Author contributions

Conceptualization: Y.W. and Z.B.L. Methodology: Z.B.L. and T.S.W. Investigation: Z.B.L. Visualization: Z.B.L. Supervision: Y.W. and L.S.H. Writing—original draft: Z.B.L. Writing—review & editing: Y.W., Y.-G.Z. and H.F.Q.

Competing interests

The authors declare no competing interests.

Additional information

Supplementary information The online version contains supplementary material available at <https://doi.org/10.1038/s41467-025-63808-1>.

Correspondence and requests for materials should be addressed to Yong Wang.

Peer review information *Nature Communications* thanks Lois Maignien, Ri-Qing Yu, and the other anonymous reviewer(s) for their contribution to the peer review of this work. A peer review file is available.

Reprints and permissions information is available at <http://www.nature.com/reprints>

Publisher's note Springer Nature remains neutral with regard to jurisdictional claims in published maps and institutional affiliations.

Open Access This article is licensed under a Creative Commons Attribution-NonCommercial-NoDerivatives 4.0 International License, which permits any non-commercial use, sharing, distribution and reproduction in any medium or format, as long as you give appropriate credit to the original author(s) and the source, provide a link to the Creative Commons licence, and indicate if you modified the licensed material. You do not have permission under this licence to share adapted material derived from this article or parts of it. The images or other third party material in this article are included in the article's Creative Commons licence, unless indicated otherwise in a credit line to the material. If material is not included in the article's Creative Commons licence and your intended use is not permitted by statutory regulation or exceeds the permitted use, you will need to obtain permission directly from the copyright holder. To view a copy of this licence, visit <http://creativecommons.org/licenses/by-nc-nd/4.0/>.

© The Author(s) 2025